1.4 *MESOSCALE PROCESSES AND ENERGETICS OF FASTEX SECONDARY CYCLOGENESIS (IOPs 1, 11, 12, 16, 17)*

C. HEYRAUD*, A. PROTAT*, and Y. LEMAITRE*
Centre d'Etude des Environnements Terrestre et Planétaires (CETP), Vélizy, France

1. INTRODUCTION

During FASTEX (January and February 1997) , 19 frontal cyclones at different stages of development have been sampled using airborne facilities (dropsondes and 2 dual-beam Doppler radars). Thanks to this important data set, the three-dimensional dynamic and microphysical structure of the North–Atlantic frontal cyclones is documented and the multi-scale processes are investigated in the present paper. Previous studies conducted at CETP on a bent-back warm front case of FASTEX (Intensive Observing Period 16, IOP16) documented the dynamic and thermodynamic structure at all scale of motions. Hypotheses deduced from recent theoretical studies of the dynamics of frontal cyclones have been evaluated. In this context, the conceptual scheme of secondary cyclones of Browning (1997) has been validated. Bouniol *et al* (2001) underscore the crucial role played by specific mechanisms in the intensification of this typical secondary low:

- upper and low level coupling processes (see for instance Thorncroft and Hoskins (1990)).
-low forcing of the large scale environment (see for instance Bishop and Thorpe (1994a, b)).
- instability mechanisms: conditional symmetric instability (see for instance Balasubramian and Yau (1994)).
-vorticity aspect: importance of vorticity stretching in vorticity production at the low center.

This study also evidenced the very complex cloud vertical stratification and energetic structure.
The present study attempts to evaluate the degree of generality of these results. For this purpose, 4 cases at different stages of development are investigated.
This study is based on the estimation of diagnostic parameters at mesoscale, such as production of vorticity, energetic conversion, and impact of cyclogenesis on the environment in terms of heat budgets. All these points are discussed below.

* *Corresponding author address:*
Catherine Heyraud, CETP/CNRS, 10/12 avenue de l'Europe, 78140 Vélizy, France;
e-mail: catherine.heyraud@cetp.ipsl.fr

2. DATA AND METHODS

The measurement have been collected by two aircraft (NOAA P-3 and NCAR Electra, Fig. 1) bearing the airborne Doppler radars and the C-130 aircraft from which dropsondes were launched every 70km within the cyclones.

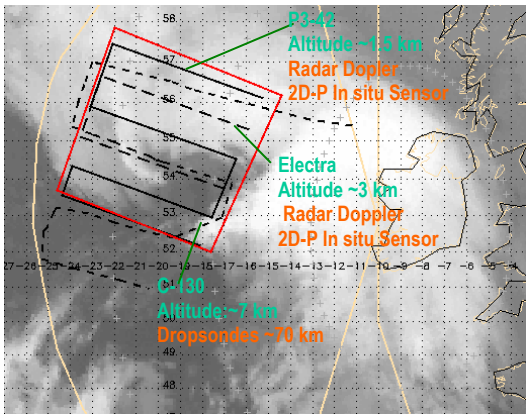

Fig 1: IOP1 sampling strategy overlayed on the Meteosat IR image at 06 UTC. The 3 flight tracks are represented in the mesoscale retrieval MANDOP box near the Irish coast.

The combination of the measurements allows to document the three-dimensional wind field in both the precipitating and non-precipitating areas of the cyclone using the MANDOP analytical method (Scialom and Lemaître 1990) adapted by Montmerle and Lemaître (1998) to include the dropsonde information in the variational process. The 3-D thermodynamic fields (pressure and temperature) are retrieved using the analytical method developed by Protat et al. (1998). The water vapor field is retrieved using the dropsonde measurements (Bouniol et al. 1999).

3. SELECTED FASTEX CASES

During FASTEX different kinds of meteorological events have been sampled from the weak frontal wave to the explosive cyclogenesis (Shapiro and Keyser 1990). The IOP16 sampled on the 17 February 97 is a fast moving rapidly-deepening secondary wave with emerging cloud

head and distinct dry intrusion. Three other cases have been selected to conduct this study: IOP1, IOP11, IOP17.

IOP1 (10 January 97) is a frontal fracture, the cloud head and dry intrusion are observed. IOP17 (19 February 1997) is the "FASTEX CYCLONE", this is an explosive deepening cold wave characterised by a 40 mb deepening in 24 hours. IOP11 (5-6 February 1997) is a deepening primary cyclone with training cold and warm fronts.

The dynamic and thermodynamic characteristics of these frontal cyclones have been retrieved. Thanks to this important data set, the ambition addressed is to extend the characteristics revealed on the IOP 16 case by scrutinizing the four selected FASTEX cases.

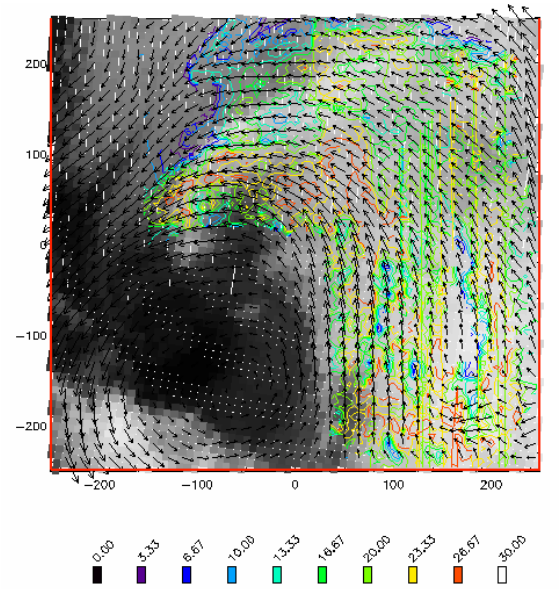

Fig 2: IOP1 reflectivity contour and wind field in the MANDOP retrieval box overlayed on the Meteosat IR image at 06 UTC.

4. PRODUCTION OF VORTICITY

The purpose of this section is to evaluate the evolution of the cyclogenesis and to diagnose the processes involved in this evolution in terms of the absolute vorticity :

$$\vec{\omega_a}=\vec{\nabla}\wedge\vec{V}+f\vec{k}=\eta\vec{i}+\xi\vec{j}+(\zeta+f)\vec{k} \qquad (1)$$

$$\frac{D(\quad f)}{Dt}=\eta\frac{\partial w}{\partial x}+\xi\frac{\partial w}{\partial y}+(\zeta+f)\frac{\partial w}{\partial z}+$$

$$\frac{\partial F_y}{\partial x}-\frac{\partial F_x}{\partial y}-\frac{1}{\rho^2}\left(\frac{\partial\rho}{\partial x}\frac{\partial p}{\partial y}-\frac{\partial\rho}{\partial y}\frac{\partial p}{\partial x}\right)-(\zeta+f)\frac{\vec{\nabla\rho}}{\rho}.\vec{V} \qquad (2)$$

Where (u,v,w) are the wind components, (η,ξ,ζ+f) are the absolute vorticity components, f is the coriolis parameter, F is the friction and ρ the density. The quantification of the different terms of this equation indicates that only the stretching $(\zeta+f)\frac{\partial w}{\partial z}$ and tilting $(\eta\frac{\partial w}{\partial x}+\xi\frac{\partial w}{\partial y})$ terms have significant values (first and second terms of (2)). The other terms are negligible. The mean vertical profiles are computed in a 170*170km² box centred on the maximum vorticity. This box is located in the cyclonic circulation area observed in the low tropospheric layers (1.5km).

Fig 3 shows the vertical component of vorticity for the four IOPs. For all the cases it is positive and the maximum (3-4 10^{-4} s^{-1}) is located at around 1 km altitude. This result confirms the presence of an intense cyclonic circulation in this area.

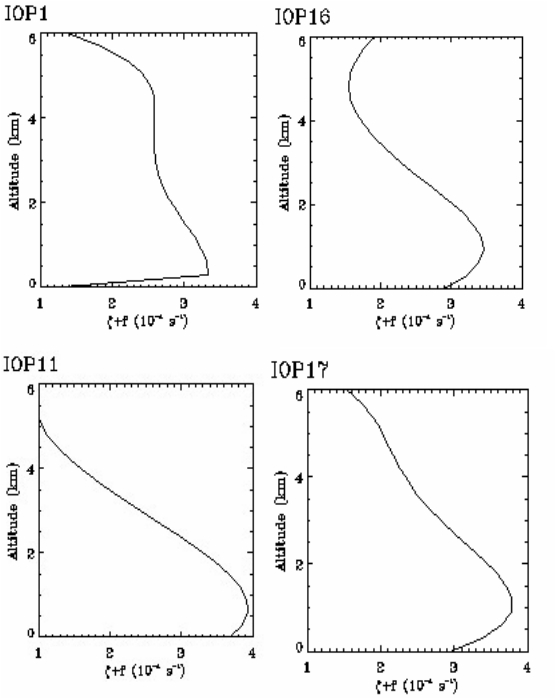

Fig 3: Mean vertical profile of the vertical vorticity component ($10^{-4}s^{-1}$)

The quantification of the different components of (2) allows to diagnose the processes involved in the evolution.

Fig 4 shows the Lagrangian evolution of this parameter and the stretching term.

IOP1

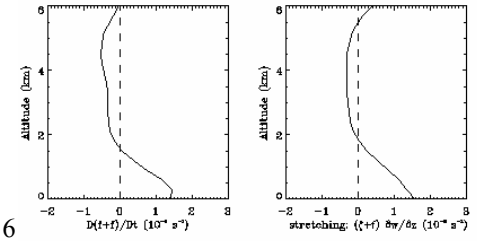

IOP16

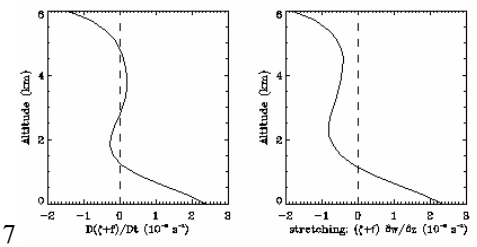

IOP17

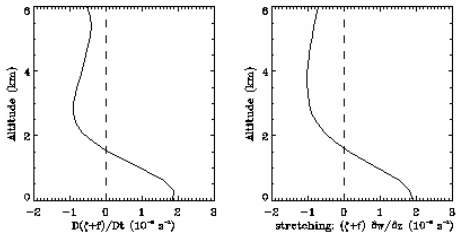

IOP11

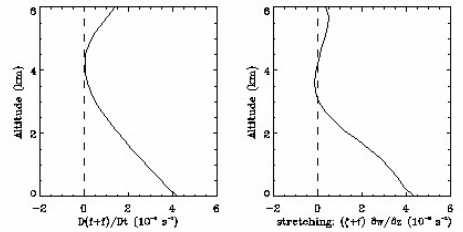

Fig 4: Mean vertical profile of the vorticity evolution (first column) and stretching term (second column) for IOPs 1,16,17,11. ($10^{-8}s^{-1}$)

These figures highlight that there is a production of vorticity in the low tropospheric layers (below 2 km altitude) for the 4 cases. The vorticity production typically varies from 1 to 2 $10^{-8}s^{-1}$, except for IOP11 case, for which the production is two times larger. An explanation could be that the stage of development of IOP11 is less advanced than the other cases. As shown by the strong similarity of the production and the stretching term profiles in Fig. 4, the evolution of vorticity is mostly driven by the stretching term.

5. ENERGETIC CONVERSION

The aim of this section is to answer the following question: what are the instabilities and the conversion mechanisms systematically involved in the development of secondary cyclogenesis? What are their origins?

The production /dissipation of kinematic energy is governed by different processes :

$$\frac{\partial E_c}{\partial t}=\frac{g}{\theta_0}\overline{w'\theta'}-\frac{1}{\rho}\overline{\vec{V}.\vec{\nabla}p'}-\overline{(u'+v'+w')\vec{V}'.\vec{\nabla}(\bar{u}+\bar{v}+\bar{w})}-\overline{\vec{V}.\vec{\nabla}E_c} \qquad (3)$$

Where the over-bar denotes the average over the whole retrieval domain and the prime denotes the deviation from the average. □ is the potential temperature, the wind vector V component are (u,v,w).

The first term on the right hand side of (3) is the vertical heat flux, the second term the production due to the pression term, the third term the Reynolds Stress (RS) and the last one the advection term. The Reynolds Stress reveals the energy exchange between the different scales: larger and "perturbation" scale by means of energetic conversion associated with conditional symmetric instability (CSI) and barotropic instability. These terms can be expressed as in (4). The first term of (4) relates to the horizontal Reynolds Stress (HRS) relevant to the presence of CSI and the second the vertical Reynolds Stress (VRS) relevant to the barotopic instability.

$$RS=\left[\overline{u'u'}\frac{\partial\bar{u}}{\partial x}+\overline{v'v'}\frac{\partial\bar{v}}{\partial y}+\overline{u'v'}\left(\frac{\partial\bar{u}}{\partial y}+\frac{\partial\bar{v}}{\partial x}\right)+\overline{u'w'}\frac{\partial\bar{w}}{\partial x}+\overline{v'w'}\frac{\partial\bar{w}}{\partial y}\right]+$$

$$\left[\overline{u'w'}\frac{\partial\bar{u}}{\partial z}+\overline{v'w'}\frac{\partial\bar{v}}{\partial z}+\overline{w'w'}\frac{\partial\bar{w}}{\partial z}\right] \qquad (4)$$

Fig 5 shows the HRS and VRS vertical profiles for the four IOPs calculated in the previous 170 km^2 box.

From these figures it is clearly seen that in the low layer of atmosphere the positive tendency of the horizontal Reynolds stress overheads the presence of barotropic conversion of energy, while at higher height there is a clear signature of conversion conducted by CSI.

IOP1

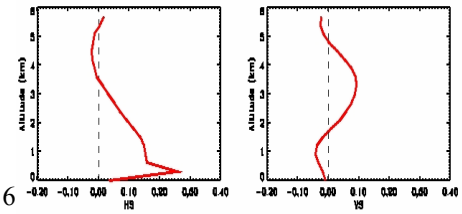

IOP16

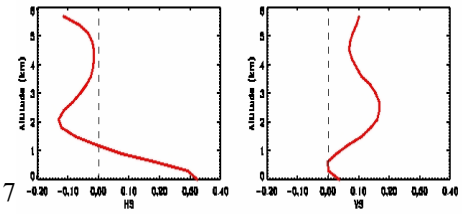

IOP17

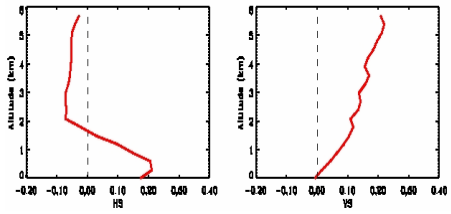

IOP11

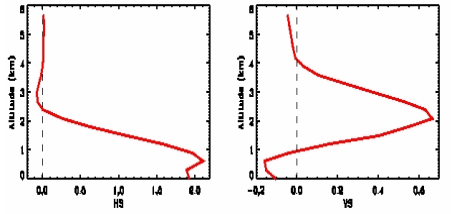

Fig 5: Mean vertical profile of HRS (first column) and VRS (second column) (10^{-2}J.kg^{-1}s^{-1}) for IOPs 1, 16, 17, 11.

6. HEAT BUDGET OF THE CYCLONES

In this section, the impact of cyclogenesis on the environment is quantified in terms of net heating/cooling using the apparent heat budget (Q_1) :

$$Q_1 = \bar{\pi}(V - C).\nabla\bar{\theta} \qquad (5)$$

where π is the nondimensional pressure, θ the potential temperature, C the advection speed vector of the moving frame of reference, and the over-bar denotes the average over the whole retrieval domain. This equation may also be rewritten as:

$$Q_1 = -\frac{\bar{\pi}}{\bar{\rho}}\bar{\nabla}.(\bar{\rho}\theta\vec{V}_r) + \bar{\pi}S(\bar{\theta}) + D_{Q_1} \qquad (6)$$

where the prime denotes the deviation from the average, D_{Q1} is a subgrid-scale diffusion term (computed in the present case but always negligible), and $S(\theta)$ is a source term reflecting diabatic heating.

The first term on the right-hand side of (4) is the eddy heat flux convergence term, reflecting warming/cooling of the environment of the cyclone due to scales resolved by the analysis or smaller. An estimate of the latent heat term is obtained by computing the eddy heat flux convergence term in (4) and subtracting it to the Q_1 computed using (3).
In this section, the IOP12 case is also studied.
IOP12 is an explosive cyclogenesis case, with well-developed cloud head and dry slot features, and an organised line of thunderstorms.

The mean vertical profile of Q1 is depicted in the mesoscale area (Fig 6).

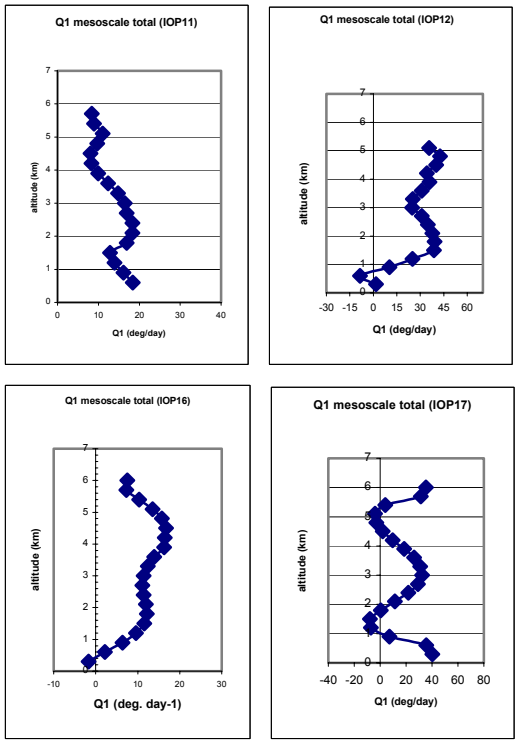

Fig. 6: Vertical profile of the heat source on mesoscale for IOPs 11, 12, 16, and 17.

The positive tendency of the apparent heat budget indicates that the cyclogenesis tends to stabilize the atmosphere through warming. The heating intensity appears to be related to the intensity of the cyclone. For instance IOP12 and IOP17 defined as the most intense FASTEX cyclogeneses result in the strongest warming (30-40K/day).

Signatures of cooling are also identified in the low layers of the troposphere except for IOP11 that is still in a development stage. This cooling plays a part below 1km altitude for IOP12 and 16 and between 1 and 2 km for IOP17.

All these points indicates that there is no “typical” profile of Q1. The shapes of the profiles seem to be related to the stage of development and the structure of the cyclogenesis (presence of cloud head), but we do not have enough cases to confirm this conclusion unambiguously.

7. CONCLUSION

These first results show the existence of systematic behaviour of secondary cyclogenesis in terms of production of vorticity, energetic conversion and global impact on the environment (even if there is no typical vertical profile of Q1).

The estimate of diagnostic parameters will be also obtained on another FASTEX case (IOP5). However our short-term perspective is to widen this study on other diagnostic parameters such as potential vorticity, moist potential vorticity, impact of cyclogenesis on the environment in terms of momentum and moisture budget.

References

Balasubramian, G. and M. K. Yau, 1994: Baroclinic instability in a Two-layer Model with Parametrized Slantwise Convection. *J. Atmos. Sci.*, 26, 570-583.

Bishop, C. H. and A. J. Thorpe, 1994b: Frontal wave stability during moist deformation frontogenesis. Part II: The suppresion of non-linear wave development. *J. Atmos. Sci.*, 51, 873-888.

Bouniol, D., A. Protat, and Y. Lemaître, 1999: Mesoscale dynamics of a deepening secondary cyclone (FASTEX IOP16): Three-dimensional structure retrieved from dropsonde data. *Quart. J. Roy. Meteor. Soc.*, 125, 3535-3562.

Bouniol, D., Y. Lemaître and A. Protat, 2001 : Upper and lower tropospheric coupling processes involved in the FASTEX IOP16. *Quart. J. Roy. meteorol. Soc.*, submitted.

Browning, K. A., and N. M. Roberts, 1994 : Structure of a frontal cyclone. *Quart. J. Roy. Meteor. Soc.*, 120, 1535-1557.

Browning, K. A., 1997: Mesoscale aspects of extratropical cyclones: an observational perspective. Bergen post-conference book. ED. M. Shapiro. American Meteorological Society, Boston, Mass.

Emanuel, K. A., M. Fantini and A. J. Thorpe, 1987 : Baroclinic instability in an environment of small slantwise convection. Part I : Two-dimensional models. *J. Atmos. Sci.*, 44, 1559-1573.

Joly, A., and Co-authors, 1997: The Fronts and Atlantic Storm-Track Experiment (FASTEX): scientific objectives and experimental design. *Bull. Am. Meteor. Soc*., 78, (9), 1917-1940.

Lemaître, Y., A. Protat, and D. Bouniol, 1999: Pacific and Atlantic "bomb-like" deepenings in mature phase: A comparative study. *Quart. J. Roy. Meteor. Soc.*, 125, 3513-3534.

Montmerle, T, and Y. Lemaître, 1998: 3D variational data analysis to retrieve thermodynamical and dynamical fields from various nested wind measurements. *J. Atmos. Oceanic Technol.,* 15, 360-379.

Protat, A., Y. Lemaître, D. Bouniol, and R. A. Black, 2000: Microphysical observations during FASTEX from airborne doppler radar and in-situ measurements. Phys. Chem. Earth (B), 25, 1097-1102.

Scialom, G., and Y. Lemaître, 1990: A new analysis for the retrieval of the three-dimensional wind field from multiple Doppler radars, *J. Atmos. Oceanic Technol.,* 7, 640-665.

Shapiro, M. A., and D. Keyser, 1990: Fronts, jet-streams and Tropopause. In Extratropical cyclones: the Erik Palmen Memorial Volume, C.W Newton and E.O.Holopainen, Eds. American Meteorological Society, 167-191.

Shapiro M. A. and P. J. Kennedy, 1981 : Research aircraft measurements of jet-stream geostrophic winds. *J. Atmos. Sci*., 117, 2447-2462.

Thorncroft, C. D. and B. J. Hoskins, 1990: Frontal cyclogenesis. *J. Atmos. Sci.*, 47, 2317-2336.